UV spectra of benzene isotopomers and dimers in helium nanodroplets

Roman Schmied,[a] Pierre Çarçabal,[b] Adriaan M. Dokter,[c] Vincent P. A. Lonij,
Kevin K. Lehmann, and Giacinto Scoles
Department of Chemistry, Princeton University, Princeton, New Jersey 08544

We report spectra of various benzene isotopomers and their dimers in helium nanodroplets in the region of the first Herzberg-Teller allowed vibronic transition $6_0^1\ ^1B_{2u} \leftarrow\ ^1A_{1g}$ (the A_0^0 transition) at ~260 nm. Excitation spectra have been recorded using both beam depletion detection and laser-induced fluorescence. Unlike for many larger aromatic molecules, the monomer spectra consist of a single "zero-phonon" line, blueshifted by ~30 cm^{-1} from the gas phase position. Rotational band simulations show that the moments of inertia of C_6H_6 in the nanodroplets are at least six-times larger than in the gas phase. The dimer spectra present the same vibronic fine structure (though modestly compressed) as previously observed in the gas phase. The fluorescence lifetime and quantum yield of the dimer are found to be equal to those of the monomer, implying substantial inhibition of excimer formation in the dimer in helium. © *2004 American Institute of Physics.* [DOI: 10.1063/1.1767515]

I. INTRODUCTION

Among all molecules, benzene occupies a very special place: it is an organic molecule, with its conjugated ring forming the basis for a vast field of chemistry; it is also effectively a very small molecule, partially owing to its high degree of symmetry, and can thus be studied with very high-resolution techniques, both theoretical[1] and experimental.[2–6] In fact, the benzene monomer and its isotopomers have been extensively studied since the 1960s, when Callomon *et al.*[7] first published a detailed analysis of moderate-resolution UV absorption spectra of room temperature benzene vapor. However, benzene van der Waals interactions with itself and other molecules,[8] which are relevant to both biochemistry and molecular electronics, have proved more demanding because of the nonrigid nature of most complexes formed with benzene. In particular, the structure and internal degrees of freedom of the benzene dimer are still not firmly established.

In the present work we have studied benzene and its dimer solvated in superfluid helium nanodroplets, in order to further our understanding of these systems. Much is known about the gentle solvation effects in helium nanodroplets,[9,10] which allows us to interpret the obtained spectra in great detail. In particular, two molecules picked up by the same helium nanodroplet will rapidly (≲1 ns) form a very cold van der Waals dimer, shedding their relative kinetic and potential energies into the droplet and reaching an equilibrium rotational and vibrational temperature of ~0.38 K. In the past, helium nanodroplet isolation (HENDI) has revealed rotationally resolved spectra[11,12] of many molecules, which has been interpreted as a demonstration of the superfluid nature of these droplets. Electronic spectra have been recorded for a

series of molecules,[13] in particular for higher polyacenes (see Table II) and other aromatic molecules. In the case of glyoxal, the observation of a characteristic gap between the zero-phonon line (ZPL) and the phonon wing provided the first direct evidence for superfluidity in helium nanodroplets.[14] The same gap was also observed for Na_2 molecules located on the surface of the droplets.[15] For many other molecules, the electronic spectra feature several "zero-phonon" lines, whose origin has been extensively discussed in the literature.[13,16–20] While benzene has not been experimentally studied in helium droplets before, several theoretical papers have appeared on this subject.[21–23]

We have focused our studies on the A_0^0 vibronic transition of benzene, which is the lowest Herzberg-Teller allowed transition to the first electronic excited spin-singlet state (S_1, a $\pi \rightarrow \pi^*$ excitation). It occurs around 259 nm, and has a long history of gas phase studies.[7] The $S_1 \leftarrow S_0$ transition is symmetry forbidden, but simultaneously exciting one quantum of the asymmetric ring breathing vibrational mode ν_6 (521.4 cm^{-1} for C_6H_6 in the gas phase)[24] breaks the sixfold symmetry (Herzberg-Teller coupling) and makes this vibronic transition allowed by perpendicular-band one-photon absorption. Higher transitions in the A_n^0 sequence include simultaneous excitation of n quanta of the totally symmetric ν_1 vibration (923.538 cm^{-1} for C_6H_6 in the gas phase, see Table I). The absorption oscillator strengths of the lowest few A_n^0 transitions are on the order of only 1×10^{-4} (Refs. 25 and 26), which has posed a significant experimental challenge.

The isotopomers examined in this study were C_6H_6, C_6H_5D, s-$C_6H_3D_3$ and C_6D_6, and their homodimers. Excitation spectra were recorded both in helium droplet beam depletion using bolometric beam flux detection, and in laser-induced fluorescence excitation. The former method, ideally suited for poorly fluorescent species,[27] has given a better signal-to-noise ratio, on the order of 100 or less; the latter method was not as successful due to the relatively low fluo-

[a]Electronic address: rschmied@princeton.edu
[b]Present address: Laboratory of Physical and Theoretical Chemistry, Oxford University, Oxford OX1 3QZ, United Kingdom.
[c]Present address: Institute for Atomic and Molecular Physics, Kruislaan 407, Amsterdam, The Netherlands.

TABLE I. Absorption line positions of various benzene isotopomers and dimers in helium nanodroplets (beam depletion spectra). Units are cm^{-1}; uncertainties in present measurements are 0.02 cm^{-1} where not specified. Measurements are peak positions of least-squares fitted Gaussians. The measurement in square brackets refers to the band origin of a fitted spectrum (see Fig. 4). Energies labeled with an asterisk have been adjusted with more accurate values of the respective monomer transitions (see text).

Molecule	Line	Droplet	Gas phase	Ref.	Shift
C_6H_6	A_0^0	38636.47	38606.098(2)	6	+30.37
		[38636.41]			[+30.31]
C_6H_5D	$A_{0(a)}^0$	38664.85	38634.2429(1)	79	+30.61
	$A_{0(b)}^0$	38667.67	38637.1792(1)	79	+30.49
s-$C_6H_3D_3$	A_0^0	38725.98			
C_6D_6	A_0^0	38817.12	38785.935(10)	63	+31.19
$(C_6H_6)_2$	A_0^0	38599.34	38561.9*	45	+37.4*
			38563.0*	44	+36.3*
		38602.24	38565.6*	45	+36.6*
			38566.7*	44	+35.5*
$(C_6H_5D)_2$	A_0^0	38628.28			
		38629.65(6)			
		38630.35(3)			
		38630.99(8)			
		38632.95			
		38633.51			
$(s$-$C_6H_3D_3)_2$	A_0^0	38688.43			
		38690.44(3)			
		38691.20			
		38692.13			
$(C_6D_6)_2$	A_0^0	38779.49	38741.7*	44	+37.8*
		38781.65(3)			
C_6H_6	A_1^0	39560.73	39529.636(3)	80	+31.10
$(C_6H_6)_2$	A_1^0	39521.09(3)			
		39523.85			
		39526.37			
C_6H_6-Ar	A_0^0	38619.27	38585.071(8)	61	+34.20

rescence yield of benzene (~20%).[28] It was sufficient, however, for measuring the fluorescence lifetimes of C_6H_6 and $(C_6H_6)_2$ in helium nanodroplets.

II. EXPERIMENT

The apparatus is described in detail elsewhere.[12,29] In brief, helium droplets are produced in a supersonic expansion at 59 bar of research grade ^{4}He (99.9999%, Ref. 30) through a 10 μm nozzle at 14 K, and pass through a 390 μm skimmer into the experimental chamber. Under these conditions, the droplets have an average size of about 35 000 atoms (extrapolating from the data of Ref. 31). Bolometric intensity measurements with a chopped cluster beam yield ~2.5×10^{14} helium atoms striking the detector per second. Assuming 50% clusterization and the above mean cluster size, we estimate a total flux of ~4×10^9 helium nanodroplets per second. The droplets are doped while crossing a 2 cm pickup cell, in which benzene is present at a pressure, on the order of 10^{-4} mbar, which can be optimized for a single or double pickup. After doping they interact with a frequency-tripled kilohertz pulsed Ti:Al$_2$O$_3$ laser in a wedged dielectric mirror multipass (98% reflective) with about 40 beam crossings. A high repetition rate laser, combined with a multipass cell, provides an acceptable duty cycle of about 5% cluster beam illumination, with the advantage of easy access to

higher harmonics. The beam flux is detected with a silicon bolometer attached to a 3×3 mm^2 sapphire slab,[32] with a noise-equivalent power of 0.13 pW/$\sqrt{Hz}$. A collimator measuring 4 mm in diameter limits the cluster beam access to the sapphire slab. The distance between the skimmer and the bolometer is ~35 cm. Evaporation of the helium droplets following resonant excitation of benzene molecules is measured by chopping the pulsed laser beam at the fourth subharmonic of the laser repetition rate and amplifying the bolometer signal through a cold J230 JFET,[32] a Stanford SR550 preamplifier, and a SR510 lock-in amplifier. Detection at the repetition rate of the laser could not be used due to the relatively slow response of the bolometer and the high minimum repetition rate of the pump laser.

The Ti:Al$_2$O$_3$ laser is a prototype Indigo[33] system with a Fox-Smith resonator,[34] pumped by an Evolution-30 (Ref. 33) diode-pumped intracavity-doubled Nd:YLF laser. It provides relatively narrow-band [~0.1 cm^{-1} full width at half maximum (FWHM)] infrared pulses of ~10 ns duration at up to 3 kHz repetition rate. Second-harmonic light was generated in a lithium triborate (LBO) crystal, and combined with the fundamental in a beta barium borate (BBO) crystal to produce third-harmonic radiation in the 260 nm region, with an estimated linewidth of 0.2 cm^{-1} FWHM. The wavelength of the Ti:Al$_2$O$_3$ fundamental was measured with a Burleigh

WA-4500 pulsed wavemeter,[35] and a Fe-Ne hollow-cathode lamp provided absolute calibration at the second harmonic. We estimate our wavelength calibration to be accurate to 0.02 cm^{-1} and precise to 0.01 cm^{-1}. For all measurements, the laser was running at a repetition rate of 1083 Hz, with a typical UV pulse energy of 30 μJ.

Fluorescence excitation spectra were acquired with a Hamamatsu[36] H5783-04 photomultiplier tube (PMT), which has a cathode radiant sensitivity of about 40 mA/W at 250 nm, corresponding to a quantum efficiency of $\sim 20\%$. The PMT was mounted at $90°$ from the cluster and laser beams, and on the order of 50% of the fluorescence photons were collected with a hemispheric/ellipsoidal aluminum mirror assembly.[37] The gain of the PMT was estimated at $\sim 2 \times 10^6$ by single-photon observation on a fast oscilloscope. After dropping the collector current over a 50 Ω terminator, the PMT output was integrated for 20 ns (for lifetime measurements) or 50 ns (spectra) with a SR250 boxcar integrator, and the result fed into a SR510 lock-in amplifier locked to the laser beam chopper. The laser beam was chopped to eliminate the effect of electrical pickup from firing of the laser Q-switch.

All spectra were measured with 1 Hz bandwidth on the lock-in amplifier, and recorded through a computer interface with 1 Hz sampling rate. Typical scanning speeds were on the order of 1 cm^{-1}/min. The resulting data (pairs of wavelength and signal amplitude) were Gaussian smoothed with a standard deviation of 0.1 cm^{-1}.

In all isotopomers of benzene we used, carbon isotopes were present at natural abundances. C_6H_5D (98+%) and s-$C_6H_3D_3$ (sym-benzene-d_3, 1,3,5-$C_6H_3D_3$, 98%) were purchased from Aldrich;[38] C_6D_6 (99.5%) was purchased from Cambridge Isotope Laboratories.[39] All isotopomers were used without further purification. A ^{1}H NMR spectrum of a C_6H_6 / C_6D_6 mixture showed no significant impurities.

III. BEAM DEPLETION SPECTRA

The recorded beam depletion spectra were assigned by studying line intensities as functions of the dopant pressure in the pickup cell, verifying the typical Poisson distribution expected for uncorrelated pickup events.[40] We will present and discuss the spectra in five sections, separately considering the line shapes of the monomer, those of the dimer, the complexes with argon, the droplet solvation shifts, and the excitation of a totally symmetric vibrational mode.

A. Monomer spectra

The A_0^0 absorption lines of all the benzene monomer isotopomers we have studied were found to present the same vibronic fine structure as in the gas phase, consisting of a single absorption line within our experimental resolution (two lines in the case of C_6H_5D see Fig. 1). Figure 2 shows the A_0^0 beam depletion spectrum of C_6H_6 with a signal-to-noise ratio of ~ 100; the linewidth is 0.53 cm^{-1} FWHM and the peak is at $38\,636.47$ cm^{-1}. No phonon wing was detected within 15 cm^{-1} to the blue of the transition, and we estimate that at least 90% of the spectral intensity is in the zero-phonon line. It has been shown for a variety of molecules that droplet phonon wings are often weak and require signifi-
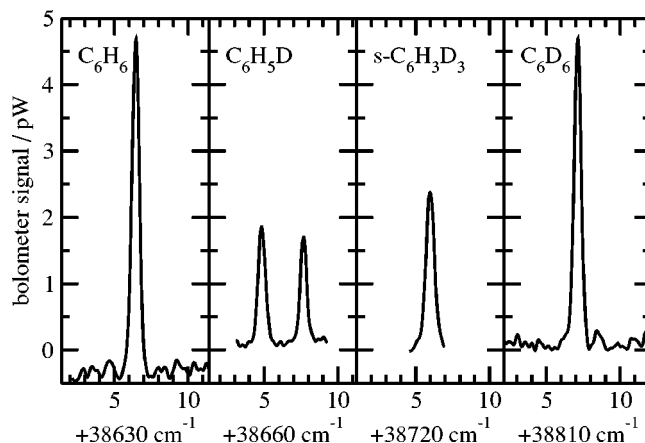

FIG. 1. Beam depletion spectra of C_6H_6, C_6H_5D, s-$C_6H_3D_3$, and C_6D_6 (left to right) in helium droplets. The peak positions are given in Table I.

cant saturation of the ZPL in order to be evident (see Ref. 13 for a review). As our conditions are far from saturation (see Sec. V), and the $\pi \rightarrow \pi^*$ valence excitation of benzene is relatively weakly coupled to the first helium solvation shell (see Sec. III D), our inability to detect a phonon wing can be rationalized.

Diffusion Monte Carlo (DMC) studies of the C_6H_6-He_{14} system have predicted a multitude of excited states of the first helium solvation shell with energies of 10–20 cm^{-1} (Ref. 22). However, UV transitions to helium excited states as computed in Ref. 22 are symmetry forbidden: helium excitations must be of A_{1g} symmetry to be excited in the A_0^0 transition,[41] which is mutually exclusive with the POITSE (projection operator, imaginary time spectral evolution) method of Ref. 22. Therefore, any helium states computed in Ref. 22 are invisible in direct UV spectroscopy, and any A_{1g} phonons that we could potentially detect are not computable with POITSE. However, the energy of the $(L,M)=(2,0)$ phonon, which can in principle be excited in the A_0^0 transition, is unlikely to be very different from that of the other $L=2$ phonons computed in Ref. 22 ($\sim 12\,k_B K$), judging
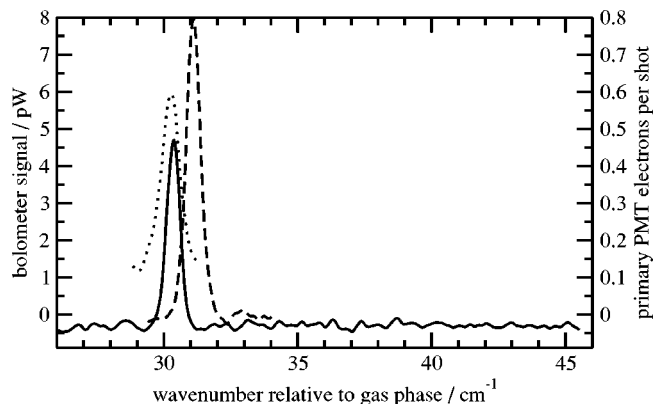

FIG. 2. Beam depletion spectra of the A_0^0 (solid) and A_1^0 (dashed) lines of C_6H_6 in helium droplets. Wave numbers are relative to the gas phase transitions (see Table I). No phonon wing is seen within 15 cm^{-1} of the A_0^0 transition. The dotted line is a fluorescence excitation spectrum of the A_0^0 transition, with the intensity (right-hand scale) referring to the estimated number of primary electrons in the photomultiplier tube per laser shot.
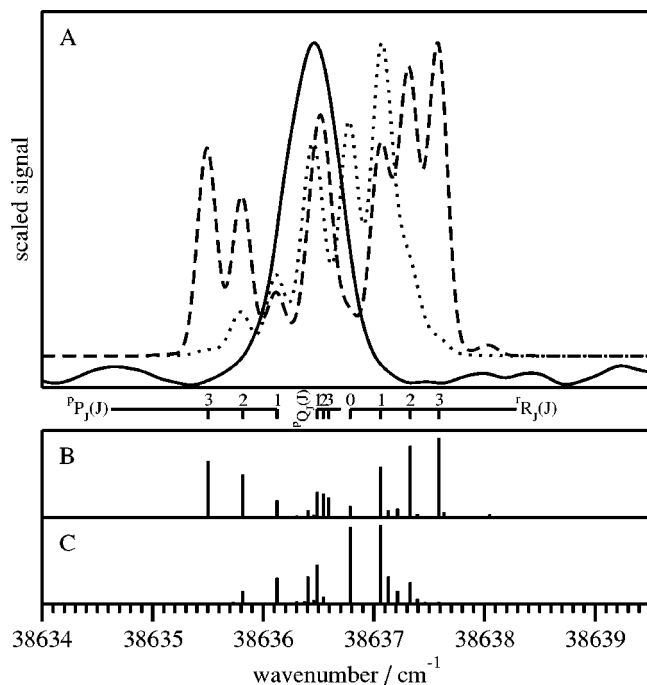
FIG. 3. Panel a: comparison of the $C_6H_6 A_0^0$ droplet spectrum (solid line) and the gas phase spectrum at 0.38 K (dashed line, from Ref. 6; convoluted with a 0.2 cm^{-1} FWHM Gaussian and shifted by $+30.31$ cm^{-1}; stick spectrum in panel b). The low-temperature populations are mostly due to the conservation of nuclear spin, as the comparison to a spin-relaxed spectrum (dotted line; stick spectrum in panel c) shows. At zero temperature, only states with $J=K\leqslant 3$ are populated.
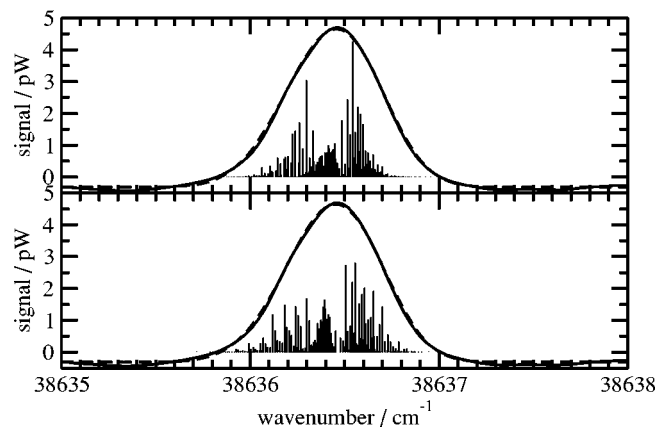

FIG. 4. Fits (dashed lines) of the $C_6H_6 A_0^0$ beam depletion spectrum (solid lines) at 0.38 K, using the rotational Hamiltonian of Ref. 6. The rotational constants B'' and B' are scaled by a numerical factor κ_B; C'' and C' (including $C_0'\zeta'$) are scaled by κ_C. The fitting procedure optimizes κ_B, κ_C, the width of the smoothing function (Gaussian), offset, amplitude, and blueshift. In the upper panel, room-temperature nuclear spin weights were assumed; in the lower panel, the nuclear spin weights were relaxed to their values at 0.38 K. Both fits are equally good, yielding no information on the importance of nuclear spin relaxation. The stick spectra are magnified ten times; they were convoluted with Gaussians of $\sim$0.4 cm^{-1} FWHM to produce the spectral fits.

from the small M dependence of the energies of the POITSE phonons in C_6H_6-He_{14}. The energy of the $(L,M)=(0,0)$ phonon, on the other hand, cannot be inferred easily because it involves a qualitatively different helium motion, being the only phonon that varies the mean density of the helium in the first solvation shell. Pending a calculation of energies and Franck-Condon factors for these excitations, we conclude that the lack of phonon wings in our spectra are due to insufficient signal-to-noise ratios.

A comparison of the $C_6H_6 A_0^0$ droplet spectrum to a simulated gas phase spectrum at 0.38 K (the experimental rotational temperature of molecules in helium droplets),[11,12] using the Hamiltonian of Ref. 6 (up to $J''=20$), shows that the droplet spectrum is significantly compressed, suggesting that the effective moments of inertia of benzene are much larger in the droplet than in the gas phase (see Fig. 3). As shown in Fig. 4, the droplet spectrum can be approximated by introducing two scaling factors κ_B (scaling B' and B'') and κ_C (scaling C', $C_0'\zeta'$, and C'') that describe the effect of the helium droplet on the rotational motion of the benzene molecules. Smaller values of κ_B and κ_C result in narrower spectra, with less recognizable structure due to the Gaussian smoothing involved; since our spectrum consists of only one peak, any values of κ_B and κ_C extracted from line fits can only be interpreted as upper limits. In this sense, we estimate that both κ_B and κ_C are smaller than $\sim$1/6. This means that the effective moments of inertia of C_6H_6 in superfluid helium are at least six times larger than in the gas phase. While a rigid model of the first solvation shell agrees with this limit on κ_B, it overestimates κ_C: a rigid C_6H_6-He_{14} cluster, with

two helium atoms on the C_6 axis 3.3 Å from the origin and 12 helium atoms in two rings of six atoms each located 3.9 Å from the origin at an angle of 45° from the C_6 axis, estimates $\kappa_B^{rigid}\approx 0.12$ and $\kappa_C^{rigid}\approx 0.33$. Note that our upper limits on κ_B and κ_C are still only about half the size of the typical values of $\sim$1/3 for large molecules.[12] The optimized widths of the smoothing functions used to produce the fitting spectra of Fig. 4, on the order of 0.4 cm^{-1}, are significantly larger than the laser linewidth ($\sim$0.2 cm^{-1}). Many electronic spectra of molecules in helium nanodroplets have been recorded with similar linewidths,[13] while purely vibrational HENDI spectra routinely achieve a hundred times smaller linewidths.[12] In the case of benzene, the observed line profiles are close to Gaussian, with little asymmetry (see Fig. 2). Rapid vibrational relaxation in S_1 with a lifetime on the order of 10 ps could account for the observed linewidth, but it would lead to more pronounced Lorentzian line wings. Inhomogeneous broadening due to either the cluster size distribution[42] or to translational levels of the benzene molecules in the clusters[43] is expected to result in asymmetric lines.

B. Dimer spectra

Figure 5 shows the A_0^0 beam depletion spectra of all benzene homodimers considered in this study. The linewidths of all sharp features are $\sim$0.5 cm^{-1}, very similar to the 0.53 cm^{-1} linewidth of the $C_6H_6 A_0^0$ line (see Sec. III A).

For the benzene dimer in the gas phase, not only the A_n^0 vibronic progression can be observed, but the reduced symmetry in the T-shaped dimer (see below) also makes the electronic origin transition 0^0 very weakly allowed. For $(C_6H_6)_2$ in the gas phase, both the 0^0 and A_0^0 UV transitions are split, featuring two peaks of similar linewidth and an intensity ratio around 1:1.4 (see Refs. 44 and 45). The A_0^0 transition
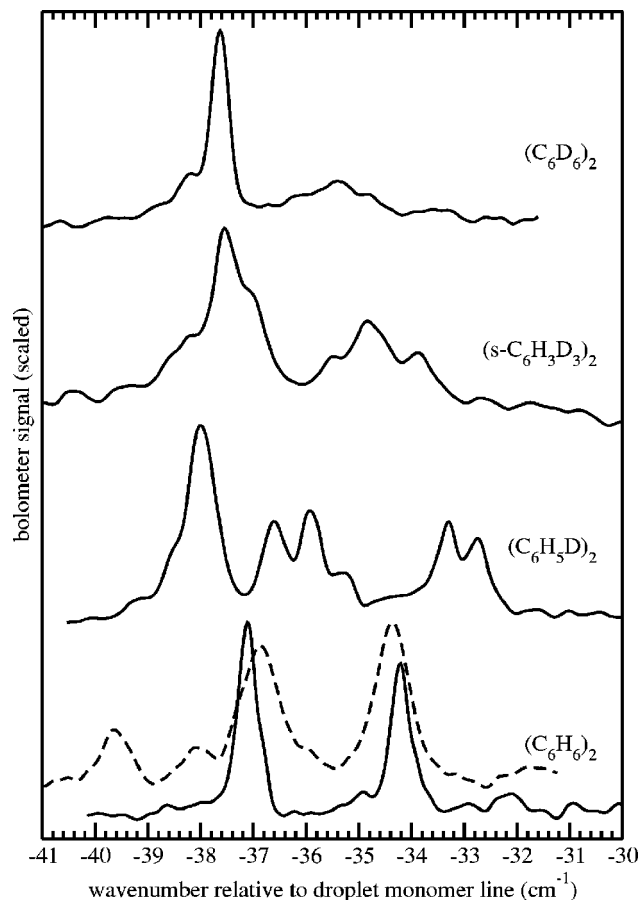
FIG. 5. Beam depletion spectra of homodimers of four benzene isotopomers in helium nanodroplets. Wave numbers are relative to the monomer absorption lines as listed in Table I [in the case of $(C_6H_5D)_2$, relative to the average of the two lines]. Solid lines are A_0^0 spectra; the dashed line is an A_1^0 spectrum.

also features a weaker progression of modes spaced by about 17 cm^{-1}, which has been assigned to the stretching of the van der Waals dimer bond.[46] While we have observed neither the 0^0 transition nor the van der Waals progression in helium droplets, the splitting of the A_0^0 transition is present in helium droplets with the same intensity ratio as in the gas phase [see
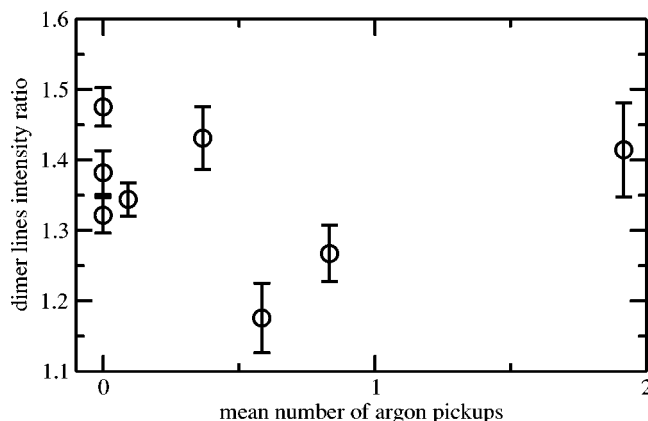

FIG. 6. Ratio of the intensity of the two $(C_6H_6)_2$ transitions as a function of argon pressure in the second pickup cell, with $\sim 8 \times 10^{-4}$ mbar resulting in one argon pickup on average. The error bars denote 1σ intervals from least-squares fits of two Gaussians and a sloped baseline to the various spectra.

Fig. 5 (lowest graph) and Fig. 6], though modestly compressed. In $(C_6D_6)_2$, the 0^0 and A_0^0 transitions were found in the gas phase to consist of a sharp line with a broader, weaker peak further to the blue,[44,45] a pattern which again was reproduced in helium droplets. Apart from a 20% smaller spacing for the two A_0^0 lines in $(C_6H_6)_2$ (3.7 cm^{-1} in the gas phase, 2.90 cm^{-1} in helium droplets), we conclude that the mechanism leading to the splitting is mostly unaffected by the helium droplet. This observation must be reconciled with the large increase in the effective moments of inertia of the individual benzene molecules in helium (Sec. III A) and the strong isotopic dependence (Fig. 5).

We will now try to establish what mechanisms can or cannot lead to the observed benzene dimer splitting; we will lead this discussion in a similar manner to that of Ref. 8, where the same issues have been discussed for the benzene dimer in the gas phase.

It was established in the gas phase work that the dimer splitting is not due to two different conformers with overlapping spectra, since the relative intensities do not depend on source conditions.[47] Further, the efficient relaxation and long-range quadrupole-quadrupole alignment[48] in helium droplets, which can align the two benzene monomers over a distance of about 30 Å, would most probably lead to intensity ratios different from those seen in jet spectra. More convincingly, hole-burning studies[46] have been able to identify two weak secondary conformers of $(C_6H_6)_2$, none of which is the source of the dimer splitting and both of which are similarly split. We have not been able to detect these conformers in helium droplets, as expected due to their smaller intensities.

Microwave spectra[49] have shown that the benzene dimer is T shaped, with a fast internal rotation around the dimer axis which leads to a symmetric-top rotational spectrum. Further arguments that favor a T shaped over a displaced-parallel dimer are (i) the perpendicular orientation of the nearest neighbors in solid benzene,[50,51] (ii) a permanent electric dipole in at least one conformer of the benzene dimer,[49,52] (iii) the demonstration that the two benzene molecules occupy inequivalent sites in the dimer,[47,53] and (iv) recent CCSD(T) (coupled-cluster singles doubles triples) (Ref. 1) and AIMI (aromatic intermolecular interaction) (Ref. 54) *ab initio* calculations. It is thus natural to suggest that the splitting is due to absorption in the two inequivalent monomers. However, studies of C_6H_6-C_6D_6 heterodimers have shown[44,46,53,55] that in both of the main A_0^0 transition lines, the "stem" monomer is almost exclusively excited, whereas the spectrum of the "top" monomer consists of an extended (~ 100 cm^{-1}) van der Waals progression with peak intensities less than 10% of those of the stem monomer. Therefore, the existence of inequivalent monomers cannot account directly for the dimer splitting.

The reduced symmetry of the stem monomer can lift the degeneracy of E-type vibrations.[56] In fact, the molecules in solid benzene do not have sixfold symmetry and their degenerate vibrational modes are split by an amount very similar to the dimer splitting.[51] While a reduced symmetry would split the A_0^0 transition (ν_6 is an E_{2g} vibration), it cannot split the nondegenerate 0^0 transition, as observed in the gas

phase. Unless the splittings of these two transitions have different origins (which is unlikely because of their qualitative similarity) we can exclude symmetry breaking as a cause for the dimer splitting. Moreover, the fluorescence lifetime of the benzene dimer in helium droplets is found to be equal to that of the gas phase monomer (Sec. IV), which would be unlikely if the stem monomer was significantly distorted since this would decrease its fluorescence lifetime. Note that a first-order perturbation of a degenerate vibronic level will result in a line doublet of equal intensities, as in the case of C_6H_5D (see Fig. 1); the very asymmetric intensity patterns observed in the dimers, in particular for $(C_6D_6)_2$, cannot be easily explained with such a symmetry-breaking mechanism.

Excitonic interactions[45,53] between the two benzene monomers can be ruled out as the source of the dimer splitting: the A_0^0 spectrum of the C_6H_6-C_6D_6 heterodimer[44,46] has been found to consist mainly of two line doublets, one doublet very similiar to the $(C_6H_6)_2$ spectrum and the other similar to the $(C_6D_6)_2$ spectrum. If the splitting was due to exciton hopping, it would be absent in heterodimers, where excitonic interactions are nonresonant.

It is interesting to note that the reduced D_{3h} symmetry of s-$C_6H_3D_3$ still allows for E-type symmetry species, resulting in a single A_0^0 absorption line (see Fig. 1). This signifies that, for most purposes related to the experiments reported here, the s-$C_6H_3D_3$ molecule can be regarded as standing halfway between C_6H_6 and C_6D_6. The sequence of $(C_6H_6)_2$, $(s$-$C_6H_3D_3)_2$, and $(C_6D_6)_2$ A_0^0 spectra show a decreasing splitting and an increasing line intensity ratio. The regularity of this progression suggests that the masses, and not the particular nuclear spin weights, of the isotopomers determine their spectra.

While tunneling of the various intermolecular motions in the dimer (librations and interchange) can lead to splittings, these are too small in magnitude and in any case limited by the associated rotational constant, which can be no larger than 0.28 cm^{-1} (for rotation around the inter-monomer axis). A tentative assignment of microwave spectra predicts small splittings of 15 or 30 kHz due to interconversion tunneling;[49] theoretical estimates of various tunneling splittings are even smaller.[1]

The most probable explanation for the dimer splitting is librational motion. A theoretical analysis[1] of the T-shaped dimer predicts intermolecular vibrational frequencies as low as 3.4 cm^{-1} for the torsion around the dimer axis (i), and 4.8 cm^{-1} for the stem rotation around its C_6 axis perpendicular to the dimer axis (ii); the interchange vibration (iii) is projected at 13.6 cm^{-1}, much larger than the observed splitting. In all of these modes, the helium solvation shell increases both the effective mass (see Sec. III A) and the curvature of the vibrational potential energy surface (one or two helium atoms are expected to localize on either side of the stem monomer,[21] further attracted to the top monomer π-cloud, thus hindering benzene dimer intermolecular motion). Sophisticated simulations, accounting for the effects of helium solvation and muclear spin statistical weights,[57,58] are called for in order to judge these assumptions.

There are two ways in which librational motion can lead to the observed dimer splittings. First, conservation of nuclear spin[59] will populate several internal-motion tunneling levels even at very low temperatures, which will have different spectra if there is a change in the intermolecular force constants upon electronic excitation. This has been conclusively ruled out as the origin of the dimer splitting by hole-burning studies[46] of the C_6H_6-C_6D_6 heterodimer. Second, excitation of a varying number of librational quanta leads to a series of absorption lines, which is what we believe is the origin of the dimer splitting.

Microwave spectra suggest that in the gas phase, the stem rotation around the dimer axis [mode (i)] has such a large zero-point motion that the T-shaped benzene dimer effectively behaves as a symmetric top; in helium droplets, however, this may not be the case since the helium strongly suppresses rotational motion, as discussed in Sec. III A. A study of selection rules and transition moments is required in order to determine which librational mode can be excited in the A_0^0 transition of the dimer.

The added complexity of the $(C_6H_5D)_2$ and $(s$-$C_6H_3D_3)_2$ spectra is most likely due to the naturally occurring different conformers. In $(s$-$C_6H_3D_3)_2$, the stem monomer can have a hydrogen or a deuterium atom pointing toward the top monomer, resulting in two slightly different conformers. Similarly, $(C_6H_5D)_2$ has four conformers depending on the orientation of the stem monomer.

C. Complexes with argon

Apart from monomer and dimer spectra of benzene, we have observed the A_0^0 spectrum of the C_6H_6-Ar dimer: Fig. 7 shows a spectrum featuring C_6H_6, C_6H_6-Ar, and $(C_6H_6)_2$ absorptions. Despite several independent attempts, no further complexes of benzene with argon were detected. In particular, we have tried to detect $(C_6H_6)_2$-Ar$_n$ and C_6H_6-Ar$_2$ complexes, in order to gain structural information of the doped helium clusters.

In the gas phase, there are two conformers of C_6H_6-Ar$_2$, with both argon atoms on the same side of the benzene plane (17 cm^{-1} redshift)[60] or on opposite sides (41.869 cm^{-1} redshift).[61] In helium droplets, as in the gas phase, the latter

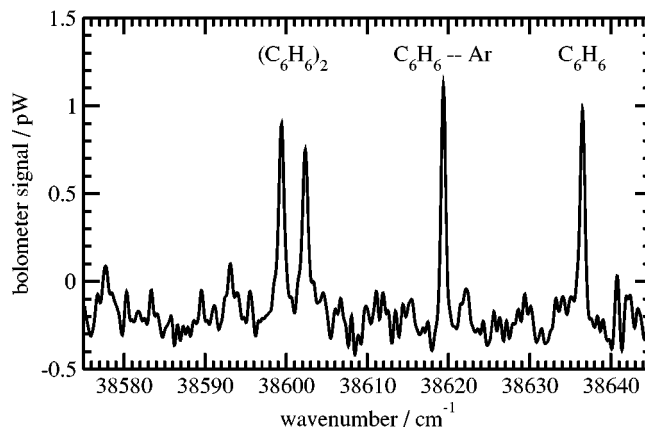FIG. 7. A_0^0 overview beam depletion spectrum of $(C_6H_6)_2$, C_6H_6-Ar, and C_6H_6. For this spectrum, a first pickup cell was filled with C_6H_6 to a pressure that resulted in equal amounts of single and double pickups, and a second cell was optimized for pickup of a single argon atom (about 8×10^{-4} mbar). No further complexes with argon were detected.

TABLE II. Solvation shifts of the electronic spectra (lowest allowed transition) of polyacenes in helium droplets.

	Molecule	Shift/cm^{-1}	ZPL[a]	Reference
	Benzene	+30.31(2)	1	This work
	Naphthalene	+15	1	81
	Anthracene	$(-38)^b$		64
	Tetracene	$-104.0(5)$	2	16
	Pentacene	$-104.0(5)$	1	16

[a]ZPL refers to the number of "zero-phonon" lines observed in helium nanodroplets.
[b]The shift for anthracene was determined with only 12 helium atoms, and is expected to be different in helium droplets.

and more stable[60] "sandwich" complex is expected to coincide[62] with the bluer one of the two $(C_6H_6)_2$ lines, since its redshift with respect to the C_6H_6 absorption line is twice that of C_6H_6-Ar, assuming the effects of the two argon atoms to be independent. A study of the dependence of the $(C_6H_6)_2$ line ratio on argon pressure in the second pickup cell (see Fig. 6) did not reveal any significant variation even for argon pressures that are optimized for about two pickups ($\sim 16 \times 10^{-4}$ mbar), where the signal of the C_6H_6-Ar_2 complex should have an amplitude comparable to that of $(C_6H_6)_2$. At this point we are unable to explain the absence of these complexes.

D. Solvation and interaction shifts

Table I lists experimental transition energies measured in helium droplets, along with the corresponding gas phase values wherever known. Previously, all dimer transition energies were given with respect to inaccurate monomer lines, which have been determined from contour fits of room-temperature spectra (see, e.g., Ref. 7) and are off by $+2.4(2)$ cm^{-1} for C_6H_6 and $+1.1(1)$ cm^{-1} for C_6D_6. The dimer transition energies listed in Table I have been computed from the more accurate monomer transitions of Refs. 6 and 63, assuming that the dimerization shifts of Refs. 44 and 45 are accurate.

Table II summarizes experimental helium solvation shifts of the smallest polyacenes, with an apparent tendency of increased redshifts with increasing molecular size. The C_6H_6 blueshift of $+30.31$ cm^{-1}, as qualitatively predicted in

TABLE III. Comparison of the electron distribution and polarizabilities in the ground (S_0) and first excited (S_1) states of C_6H_6 adapted from the CCSD calculations of Ref. 82 (Sadlej+6 basis set). Experimentally, the quadrupole moment in the ground state is $-2.1(1)$ eÅ^2 (Ref. 83) or $-1.8(1)$ eÅ^2 (Ref. 84).

	S_0	S_1
Electron charge distribution (Å^2)		
$\langle x^2 \rangle = \langle y^2 \rangle$	60.09	60.32
$\langle z^2 \rangle$	8.43	8.48
Quadrupole moment (eÅ^2)		
Q_{zz}	-1.56	-1.39
Polarizability volume (Å^3)		
$\alpha_{xx} = \alpha_{yy}$	11.96	12.30
α_{zz}	6.65	7.74

Ref. 64, agrees with previous experimental data on the A_0^0 transition of the benzene-helium system: rotationally resolved supersonic jet spectra of C_6H_6-He and C_6H_6-He_2, with the helium atoms on the C_6 axis, have found blueshifts of 2.31(2) cm^{-1} per helium atom,[2] and room-temperature spectra of benzene in high-pressure helium gas[65] have measured a ~ 10 cm^{-1} blueshift at the helium density corresponding to that of bulk liquid helium (21.8 nm^{-3}). These shifts are a combination of (i) a small dispersive redshift, due to the small polarizability of the solvating helium and the increased polarizability of benzene in the excited state (see Table III), only slightly counteracted by a decreased quadrupole moment, and (ii) a larger electronic blueshift due to the expansion of the electron cloud against the first helium solvation shell upon excitation. In fact, the helium atoms in C_6H_6-He and C_6H_6-He_2 recede from the benzene molecule by about 7–8 pm upon electronic excitation of benzene.[2] Note, however, that this expansion of the electron cloud is not reproduced in the second moments of the benzene charge distribution (see Table III), although the electronic excitation is more than halfway to the ionization threshold (74 556.57 cm^{-1}).[66] The ν_6 vibrational contribution to the droplet shift is probably much smaller than the electronic contribution, and comparable to the ν_1 vibrational droplet shift of only $+0.72$ cm^{-1} (see Sec. III E).

The $(C_6H_6)_2$ dimerization redshift (the wave number difference between the monomer and averaged dimer bands, both in helium droplets) is decreased to 35.7 cm^{-1} from the gas phase value of 42.3 cm^{-1} (Ref. 45). Similarly, the C_6H_6-Ar complexation redshift is decreased to 17.20 cm^{-1} from the gas phase value of 21.087 cm^{-1} (see Table I). These results are not easily explained: in both cases we would expect a *larger* complexation redshift in helium than in the gas phase, because (i) the adducts replace helium atoms that contributed to the 30.31 cm^{-1} blueshift of the benzene monomer, and (ii) the van der Waals bond between the adduct and the benzene monomer tends to be weakened in helium droplets with respect to the gas phase, reducing the repulsive dimerization blueshift. The latter point, suggested by a decreased exciton splitting for $(SF_6)_2$ in helium droplets,[67] is substantiated by a density-functional (DF) calculation of the C_6H_6-Ar system in a helium droplet (500 helium atoms) assuming cylindrical symmetry (Ar located on the C_6 axis of C_6H_6), using the Orsay-Paris functional,[68] with the CCSD(T) C_6H_6-He potential from Ref. 69 (averaged cylin-

drically) and the Ar-He potential from Ref. 70. At the C_6H_6-Ar equilibrium distance[71] of 3.5 Å, the DF calculation estimates a force of 1.8 pN pulling the moieties apart, resulting in a slight bond stretching of 0.5 pm (assuming a harmonic force constant of 3.5 N/m).[71]

E. A_1^0 transition

For a C_6H_6 molecule in helium nanodroplets, the wave number of one quantum of ν_1 vibration added to the ν_6 excited state of S_1 is 924.26 cm^{-1}, compared to 923.538 cm^{-1} in the gas phase (see Table I). Both ν_1 and ν_6 are mostly vibrations of the carbon ring, with the hydrogen atoms almost stationary;[72] the very small ν_1 droplet blueshift of only 0.72 cm^{-1} suggests that these modes are only weakly perturbed by the helium droplet. Moreover, in the $(C_6H_6)_2$ dimer, the shift between the center of the two main lines of the A_1^0 spectrum and the center of the A_0^0 lines (see Fig. 5) is 924.32 cm^{-1}, almost indistinguishable from the monomer value of 924.26 cm^{-1}. As we excite mostly the stem monomer in these UV transitions (see Sec. III B), the ν_1 vibration is only slightly influenced by the presence of the top monomer.

The $(C_6H_6)_2$ dimer splitting, as discussed in Sec. III B, is reduced to 2.52 cm^{-1} in the A_1^0 transition (see the lowest panel in Fig. 5). Further, an additional, weaker line is present similarly spaced to the red. In the gas phase, there are no symmetry-allowed transitions close to A_1^0 (Ref. 73). This extra line observation is then consistent with the proposed explanation of the dimer splittings through librational excitations, assuming that an additional librational excitation becomes accessible due to a modification of the van der Waals interaction in the $\nu_6 + \nu_1$ mode. If this assignment is correct, however, then the above consideration about the ν_1 energy in $(C_6H_6)_2$ becomes questionable, since we do not know which lines in the A_0^0 spectrum correspond to which in the A_1^0 spectrum.

IV. FLUORESCENCE EXCITATION SPECTRA

The fluorescence excitation spectra yielded approximately the same energies for the monomer and dimer transitions as the beam depletion spectra (see Fig. 2). The small differences are line shape distortions due to fluctuations in the laser power, since the signal-to-noise ratio of the fluorescence excitation spectra was smaller; these differences are not significant for the following discussion.

By sweeping the delay of the boxcar integrator with respect to the laser pulse, using a fixed 20 ns gate width, we determined the fluorescence lifetime of the C_6H_6 monomer to be 115(5) ns. This is comparable to the 103 ns previously reported in jet expansion experiments.[28,56] The value of 103 ns actually applies to the electronic origin (0^0) excitation, whereas we are exciting A_0^0 (gas phase lifetime: 79 ns).[28] However, the additional vibrational energy probably relaxes rapidly (much faster than 79 ns) into the helium droplet, and thus we are seeing fluorescence from the 0^0 state.

For both components of the dimer A_0^0 transition we find 120(10) ns lifetime, which is significantly longer than the gas phase value of ~40 ns (Ref. 44). The short gas phase lifetime has been attributed to a mixed state of excited van der Waals dimer and excimer[74] or the rapid conversion from the former to the latter upon excitation.[56] We therefore conclude that excimer formation of the benzene dimer is suppressed in helium droplets.

V. SIGNAL AMPLITUDES

The oscillator strengths f of the A_n^0 transitions in C_6H_6 are on the order of $(0.5–2)\times10^{-4}$ (Refs. 25 and 26). Using the measured linewidth of 0.53 cm^{-1} for the A_0^0 transition (see Fig. 2) and $f=1.37\times10^{-4}$ (Ref. 25), the peak absorption cross section is about 0.7 Å^2. A typical 30 μJ UV laser pulse with 2 mm beam diameter thus excites about 9% of the benzene molecules in its field. In a multipass cell with 98% reflectivity, 40 beam crossings thus excite a number of benzene molecules that is equal to the number of doped clusters in about 5 mm of the cluster beam (assuming no saturation effects).

The rate at which benzene molecules are excited is $\eta S/(h\nu)$, where S is the lock-in signal (converted from volts to watts through the bolometer sensitivity 2.0×10^5 V/W), $h\nu$ is the photon energy, and $\eta\approx0.2$ is the ratio of the energy it takes to evaporate a helium atom from a droplet ($\sim7\,k_BK$, Ref. 75) to the energy that this process removes from the beam flux [the kinetic energy $(5/2)k_BT_{\text{nozzle}} = 35\,k_BK$]. Complete accommodation of the cluster beam on the bolometer is assumed, which may not be accurate for our "warm" bolometer operating at 4–5 K. At a wavelength of 259 nm, a typical peak lock-in signal level of 5 pW thus corresponds to $\sim1.3\times10^6$ excited benzene molecules per second, or $\sim2.4\times10^3$ per laser pulse. This suggests that there are $\sim2.4\times10^3$ benzene-doped helium droplets in 5 mm of cluster beam (see above); since the beam moves at ~380 m/s, the total flux of benzene-doped helium clusters is estimated to be $\sim2\times10^8$ s^{-1}, or about 5% of the total number of clusters (see Sec. II), compared to $1/e$ (37%) predicted for optimal single pickup. This mismatch could be due to either an inaccurate knowledge of the mean cluster size, or the crude assumption of 50% clusterization of the helium beam.

Under the above assumptions, the first crossing of the laser with the cluster beam excites ~90 benzene molecules per shot. On the other hand, for the fluorescence signal in Fig. 2 we estimate the production of about 0.5 primary electrons in the PMT per laser shot. For this spectrum, we used a 50 ns gate delayed by about 20 ns from the UV laser pulse; this delay was necessary to avoid light scattered by the droplet beam, which was about twice as intense as the fluorescence signal. With a fluorescence lifetime of ~115 ns (see Sec. IV), we thus captured about 30% of the total fluorescence signal. Compounding this with the 20% quantum efficiency of the PMT and 50% collection efficiency, we estimate ~20 fluorescence events per laser shot.

These signal estimates yield on the order of four to five times less fluorescence events than relaxation/evaporation events per crossing of droplet and laser beams, suggesting a fluorescence quantum yield of ~20 ns, in agreement with the experimental fluorescence yield of 20% in the gas phase.[28]

Comparison of photon emission and beam depletion signals can thus be used to estimate absolute quantum yields of emission.

For the benzene dimer, the peak beam depletion signal is about half the peak monomer signal (see Fig. 5), while the fluorescence signals of monomers and dimers were found to be of similar amplitude. This indicates a larger fluorescence quantum yield for $(C_6H_6)_2$ than for C_6H_6 in helium droplets.

VI. CONCLUSIONS

Helium nanodroplet isolation electronic spectroscopy of aromatic molecules has been extended to benzene, its dimer, and its van der Waals cluster with argon, all visible in the broad scan of Fig. 7. While the cluster beam depletion spectra are very similar to gas phase spectra, they are blueshifted by about 30 cm^{-1}, confirming an apparent trend[13] of larger blueshifts for larger excitation energies in aromatic molecules (see Table II). The solvation blueshift in benzene is mostly electronic, judging from the fact that the ν_1 vibration is blueshifted by only 0.72 cm^{-1} in helium droplets.

The coupling of the electronic excitation in benzene to the surrounding helium droplet does not lead to any observable signature, and we estimate that at least 90% of the electronic absorption intensity is in the zero-phonon line.

Not surprisingly, the effective rotational moments of inertia of C_6H_6 were found to be greatly increased due to the surrounding helium. While rotational transitions could not be resolved, a contour fit estimates that the moments of inertia are larger by a factor of *at least* 6.

The splitting patterns of the A_0^0 transition in $(C_6H_6)_2$ and $(C_6D_6)_2$ are modestly compressed with respect to the gas phase, but not qualitatively altered; as their most plausible source we propose the excitation of librational intermolecular motion, although the details remain unknown. Though the spectra of $(C_6H_6)_2$ and $(C_6D_6)_2$ are substantially different, the A_0^0 spectrum of $(s\text{-}C_6H_3D_3)_2$ appears to be intermediate between the two, indicating that the dimer splitting differences are related only to the isotopic masses and not to their nuclear spin weights.

The fluorescence quantum yield and lifetime of C_6H_6 in helium nanodroplets agree with the gas phase values. The fluorescence lifetime of $(C_6H_6)_2$, however, is identical to that of C_6H_6 in helium droplets, in stark contrast to the strongly reduced lifetime of $(C_6H_6)_2$ in the gas phase. Further, the fluorescence quantum yield of the dimer was not lower than that of the monomer, contrary to gas phase studies[28,56] where it is lower by about an order of magnitude. Both the short lifetime and low fluorescence yield of the gas phase dimer have been attributed to excimer formation upon electronic excitation. In the light of our observation of sharply increased moments of inertia of benzene in helium (Sec. III A), it is likely that the transformation from the T-shaped van der Waals dimer to the excimer, which is believed to have a parallel stacked configuration,[56,76] is inhibited by the presence of helium. The fluorescence lifetime we observe would then be the lifetime of the pure van der Waals dimer, expected to be similar or slightly shorter (because of an increased internal conversion rate due to the weak van der Waals bond) than that of the monomer. We would in fact expect it to be similar to the lifetime of the trimer (81 ns, Ref. 56; 79 ns, Ref. 77), which even in the gas phase does not form an excimer.

[1] V. Špirko, O. Engkvist, P. Soldán, H. L. Selzle, E. W. Schlag, and P. Hobza, J. Chem. Phys. **111**, 572 (1999), note that the spin statistical weights in Table V contain errors for both $(C_6H_6)_2$ and $(C_6D_6)_2$; they can be computed automatically using the procedure of Ref. 58.
[2] S. M. Beck, M. G. Liverman, D. L. Monts, and R. E. Smalley, J. Chem. Phys. **70**, 232 (1979).
[3] E. Riedle, H. J. Neusser, and E. W. Schlag, Chem. Phys. Lett. **75**, 4231 (1981).
[4] M. Oldani and A. Bauder, Chem. Phys. Lett. **108**, 7 (1984).
[5] E. Riedle, T. Knittel, T. Weber, and H. J. Neusser, J. Chem. Phys. **91**, 4555 (1989).
[6] M. Okruss, R. Müller, and A. Hese, J. Mol. Spectrosc. **193**, 293 (1999).
[7] J. H. Callomon, T. M. Dunn, and I. M. Mills, Philos. Trans. R. Soc. London, Ser. A **259**, 499 (1966).
[8] S. Sun and E. R. Bernstein, J. Phys. Chem. **100**, 13348 (1996).
[9] J. P. Toennies and A. F. Vilesov, Annu. Rev. Phys. Chem. **49**, 1 (1998).
[10] Special Issue on *Helium Nanodroplets: A Novel Medium for Chemistry and Physics* [J. Chem. Phys. **115**, 10065 (2001)].
[11] M. Hartmann, R. E. Miller, J. P. Toennies, and A. Vilesov, Phys. Rev. Lett. **75**, 1566 (1995).
[12] C. Callegari, K. K. Lehmann, R. Schmied, and G. Scoles, J. Chem. Phys. **115**, 10090 (2001).
[13] F. Stienkemeier and A. F. Vilesov, J. Chem. Phys. **115**, 10119 (2001).
[14] M. Hartmann, F. Mielke, J. P. Toennies, and G. B. A. F. Vilesov, Phys. Rev. Lett. **76**, 4560 (1996).
[15] J. Higgins, C. Callegari, J. Reho, F. Stienkemeier, W. E. Ernst, M. Gutowski, and G. Scoles, J. Phys. Chem. A **102**, 4952 (1998).
[16] M. Hartmann, A. Lindinger, J. P. Toennies, and A. F. Vilesov, J. Phys. Chem. A **105**, 6369 (2001).
[17] M. Hartmann, A. Lindinger, J. P. Toennies, and A. F. Vilesov, Phys. Chem. Chem. Phys. **4**, 4839 (2002).
[18] R. Lehnig and A. Slenczka, J. Chem. Phys. **118**, 8256 (2003).
[19] M. Wewer and F. Stienkemeier, J. Chem. Phys. **120**, 1239 (2004).
[20] R. Lehnig and A. Slenczka, J. Chem. Phys. **120**, 5064 (2004).
[21] Y. Kwon and K. B. Whaley, J. Chem. Phys. **114**, 3163 (2001).
[22] P. Huang and K. B. Whaley, Phys. Rev. B **67**, 155419 (2003).
[23] M. V. Patel, A. Viel, F. Paesani, P. Huang, and K. B. Whaley, J. Chem. Phys. **118**, 5011 (2003).
[24] G. H. Atkinson and C. S. Parmenter, J. Mol. Spectrosc. **73**, 52 (1978).
[25] A. Hiraya and K. Shobatake, J. Chem. Phys. **94**, 7700 (1991).
[26] I. Borges, Jr., A. J. C. Varandas, A. B. Rocha, and C. E. Bielschowsky, J. Mol. Struct.: THEOCHEM **621**, 99 (2003).
[27] P. Çarçabal, R. Schmied, K. K. Lehmann, and G. Scoles, J. Chem. Phys. **120**, 6792 (2004).
[28] K. G. Spears and S. A. Rice, J. Chem. Phys. **55**, 5561 (1971).
[29] C. Callegari, A. Conjusteau, I. Reinhard, K. K. Lehmann, and G. Scoles, J. Chem. Phys. **113**, 10535 (2000).
[30] Spectra Gases, Inc., Branchburg, NJ.
[31] J. Harms, J. P. Toennies, and F. Dalfovo, Phys. Rev. B **58**, 3341 (1998).
[32] Infrared Laboratories, Inc., Tucson, AZ, operated as a unit gain buffer.
[33] Positive Light, Inc., Los Gatos, CA.
[34] D. J. Binks, L. A. W. Gloster, T. A. King, and I. T. McKinnie, Appl. Opt. **36**, 9371 (1997).
[35] EXFO Burleigh Products Group, Inc., Victor, NY.
[36] Hamamatsu Photonics, K.K., Hamamatsu City, Japan.
[37] U. Hefter and K. Bergmann, in *Atomic and Molecular Beam Methods*, edited by G. Scoles (Oxford University Press, New York, 1988), Vol. 1, Chap. 9, p. 242.
[38] Sigma-Aldrich Corp., St. Louis, MO.
[39] Cambridge Isotope Laboratories, Inc., Andover, MA.

[40] M. Lewerenz, B. Schilling, and J. P. Toennies, J. Chem. Phys. **102**, 8191 (1995).

[41] More precisely, the phonons must have A_{1g} or A_{2g} symmetry to be excited in the A_0^0 transition. The A_{1g} symmetry corresponds to phonons with even angular momentum L and projection $|M|=0,6,12,...$ onto the z axis defined by the benzene molecule C_6 axis; the A_{2g} symmetry corresponds to even L and $|M|=6,12,...$. Assuming that excitation of phonons with $|M|\geqslant 6$ is weak, only phonons of A_{1g} symmetry need to be considered.

[42] B. Dick and A. Slenczka, J. Chem. Phys. **115**, 10206 (2001).

[43] K. K. Lehmann, Mol. Phys. **97**, 645 (1999).

[44] K. S. Law, M. Schauer, and E. R. Bernstein, J. Chem. Phys. **81**, 4871 (1984).

[45] K. O. Börnsen, H. L. Selzle, and E. W. Schlag, J. Chem. Phys. **85**, 1726 (1986).

[46] W. Scherzer, O. Krätzschmar, H. L. Selzle, and E. W. Schlag, Z. Naturforsch., A: Phys. Sci. **47**, 1248 (1992).

[47] B. F. Henson, G. V. Hartland, V. A. Venturo, R. A. Hertz, and P. M. Felker, Chem. Phys. Lett. **176**, 91 (1991).

[48] K. Nauta and R. E. Miller, Science **283**, 1895 (1999).

[49] E. Arunan and H. S. Gutowsky, J. Chem. Phys. **98**, 4294 (1993).

[50] E. G. Cox, D. W. J. Cruickshank, and J. A. S. Smith, Proc. R. Soc. London, Ser. A **247**, 1 (1958).

[51] E. R. Bernstein, J. Chem. Phys. **50**, 4842 (1969).

[52] K. C. Janda, J. C. Hemminger, J. S. Winn, S. E. Novick, S. J. Harris, and W. Klemperer, J. Chem. Phys. **63**, 1419 (1975).

[53] B. F. Henson, G. V. Hartland, V. A. Venturo, and P. M. Felker, J. Chem. Phys. **97**, 2189 (1992).

[54] S. Tsuzuki, T. Uchimaru, K. Sugawara, and M. Mikami, J. Chem. Phys. **117**, 11216 (2002).

[55] V. A. Venturo and P. M. Felker, J. Chem. Phys. **99**, 748 (1993).

[56] J. B. Hopkins, D. E. Powers, and R. E. Smalley, J. Phys. Chem. **85**, 3739 (1981).

[57] J. A. Odutola, D. L. Alvis, C. W. Curtis, and T. R. Dyke, Mol. Phys. **42**, 267 (1981), note that Table IV contains three sign errors: line 10 of C_3C_3, line 12 of C_6C_6, and line 24 of $C_2''C_3$. Table II contains several errors as well. Permutation-group characters are easily computed with the GAP software (Refs. 58, 78).

[58] R. Schmied and K. K. Lehmann, J. Mol. Spectrosc. **226**, 201 (2004).

[59] J. Harms, M. Hartmann, J. P. Toennies, A. F. Vilesov, and B. Sartakov, J. Mol. Spectrosc. **185**, 204 (1997).

[60] M. Schmidt, M. Mons, and J. Le Calvé, Chem. Phys. Lett. **177**, 371 (1991).

[61] H. J. Neusser and H. Krause, Chem. Rev. (Washington, D.C.) **94**, 1829 (1994).

[62] T. Weber and H. J. Neusser, J. Chem. Phys. **94**, 7689 (1991).

[63] T. Weber, Ph.D. thesis, Fachbereich für Chemie, Biologie und Geowissenschaften der Technischen Universität München, 1991, as cited in Ref. 66.

[64] U. Even, I. Al-Hroub, and J. Jortner, J. Chem. Phys. **115**, 2069 (2001).

[65] R. Nowak and E. R. Bernstein, J. Chem. Phys. **87**, 2457 (1987).

[66] R. G. Neuhauser, K. Siglow, and H. J. Neusser, J. Chem. Phys. **106**, 896 (1997).

[67] M. Hartmann, R. E. Miller, J. P. Toennies, and A. F. Vilesov, Science **272**, 1631 (1996).

[68] J. Dupont-Roc, M. Himbert, N. Pavloff, and J. Treiner, J. Low Temp. Phys. **81**, 31 (1990).

[69] S. Lee, J. S. Chung, P. M. Felker, J. L. Cacheiro, B. Fernández, T. B. Pedersen, and H. Koch, J. Chem. Phys. **119**, 12956 (2003).

[70] R. Ahlrichs, R. Penco, and G. Scoles, Chem. Phys. **19**, 119 (1977).

[71] T. Brupbacher, J. Makarewicz, and A. Bauder, J. Chem. Phys. **101**, 9736 (1994).

[72] P. Pulay, G. Fogarasi, and J. E. Boggs, J. Chem. Phys. **74**, 3999 (1981).

[73] G. H. Atkinson and C. S. Parmenter, J. Mol. Spectrosc. **73**, 20 (1978).

[74] H. Shinohara and N. Nishi, J. Chem. Phys. **91**, 6743 (1989).

[75] S. A. Chin and E. Krotscheck, Phys. Rev. Lett. **74**, 1143 (1995).

[76] P. R. R. Langridge-Smith, D. V. Brumbaugh, C. A. Haynam, and D. H. Levy, J. Phys. Chem. **85**, 3742 (1981).

[77] T. Hirata, H. Ikeda, and H. Saigusa, J. Phys. Chem. A **103**, 1014 (1999).

[78] *GAP-Groups, Algorithms, and Programming, Version 4.4*, The GAP Group (2004), http://www.gap-system.org

[79] E. Riedle, A. Beil, D. Luckhaus, and M. Quack, Mol. Phys. **81**, 1 (1994).

[80] R. M. Helm, R. Neuhauser, and H. J. Neusser, Chem. Phys. Lett. **249**, 365 (1996).

[81] A. Lindinger, Ph.D. thesis, Georg-August-Universität, Göttingen, 1998, as cited in Ref. 13.

[82] O. Christiansen, C. Hättig, and P. Jørgensen, Spectrochim. Acta, Part A **55**, 509 (1999).

[83] J. Vrbancich and G. L. D. Ritchie, J. Chem. Soc., Faraday Trans. 1 **76**, 648 (1980).

[84] M. R. Battaglia, A. D. Buckingham, and J. H. Williams, Chem. Phys. Lett. **78**, 421 (1981).